p23 protects against ferroptosis of brain microvascular endothelial cells in ischemic stroke

YAO ZHAO[1-7*], YUNFEI XU[1-5*], QING XU[1-5], NINA HE[1-5], JIE ZHAO[1-5] and YING LIU[1-5]

[1]Department of Neurosurgery, Xiangya Hospital, Central South University, Changsha, Hunan 410008, P.R. China; [2]Department of Pathophysiology, School of Basic Medical Sciences, Central South University, Changsha, Hunan 410013, P.R. China; [3]Sepsis Translational Medicine Key Lab of Hunan Province, Central South University, Changsha, Hunan 410013, P.R. China; [4]National Medicine Functional Experimental Teaching Center, Changsha, Hunan 410013, P.R. China; [5]National Clinical Research Center for Geriatric Disorders, Xiangya Hospital, Central South University, Changsha, Hunan 410008, P.R. China; [6]Department of Pathology, The Sixth Affiliated Hospital, Sun Yat-sen University, Guangzhou, Guangdong 510655, P.R. China; [7]Biomedical Innovation Center, The Sixth Affiliated Hospital, Sun Yat-sen University, Guangzhou, Guangdong 510655, P.R. China

Received September 14, 2024; Accepted January 3, 2025

DOI: 10.3892/ijmm.2025.5505

Abstract. Ferroptosis is a type of iron-dependent regulated cell death that differs from apoptosis, autophagy or necrosis. p23 serves as a co-chaperone and performs a unique biological function in various diseases by binding to client proteins to modulate their biological functions; however, its effect on ferroptosis remains largely unknown. In the present study, the effects of cerebral ischemia/reperfusion (I/R) injury (CIRI) or oxygen-glucose deprivation/reoxygenation on the blood-brain barrier (BBB) and ferroptosis in brain microvascular endothelial cells (BMECs), as well as the expression of p23, were examined. Subsequently, the effects of p23 on CIRI-induced BBB dysfunction and BMEC ferroptosis were determined. Finally, the role of glutathione peroxidase 4 (GPX4) in the regulatory effects of p23 on ferroptosis was detected. The results revealed that p23 protected against BBB injury caused by CIRI by inhibiting ferroptosis in BMECs. The effect of p23 on ferroptosis was then explored, and it was found that the expression of GPX4, a major regulator of ferroptosis, was promoted by p23. Furthermore, molecular docking and co-immunoprecipitation experiments revealed that p23 could bind to GPX4 through its N-terminal domain (1-90aa), enhance the stability of GPX4 and inhibit the degradation of GPX4 by cycloheximide. Finally, a cerebral I/R animal model was established using GPX4 conditional knockout mice (GPX4 $Fos^{CreERT2/+}$), and it was revealed that the protective effect of p23 overexpression on the BBB in GPX4 $Fos^{CreERT2/+}$ mice was attenuated compared with that in GPX4 $Fos^{CreERT2/-}$ mice. In conclusion, p23 may serve a protective role against cerebral I/R-induced BBB injury by inhibiting ferroptosis in BMECs through enhancing the stability of GPX4, providing a potential therapeutic target for ischemic stroke.

Correspondence to: Dr Ying Liu, Department of Pathophysiology, School of Basic Medical Sciences, Central South University, 172 Tongzipo Road, Yuelu, Changsha, Hunan 410013, P.R. China
E-mail: liu1977ying@126.com

Dr Jie Zhao, Department of Neurosurgery, Xiangya Hospital, Central South University, 87 Xiangya Road, Kaifu, Changsha, Hunan 410008, P.R. China
E-mail: steelzj@csu.edu.cn

*Contributed equally

Key words: blood-brain barrier, cerebral ischemia/reperfusion injury, ferroptosis, glutathione peroxidase 4, p23

Introduction

Stroke is among the most prevalent causes of mortality and disability worldwide (1), and can be classified into two types, ischemic stroke and cerebral hemorrhage. At present, the principal treatment of ischemic stroke lies in restoring the blood supply to the ischemic area without delay. However, while restoring blood perfusion to the ischemic area, brain tissue damage is aggravated and leads to more serious neurological dysfunction, known as cerebral ischemia/reperfusion (I/R) injury (CIRI) (2). A pathophysiological trait of ischemic stroke is the disruption of the blood-brain barrier (BBB), characterized by increased permeability due to the breakdown of tight junctions (TJs) between brain microvascular endothelial cells (BMECs) and the increased vesicular transport in BMECs, causing unregulated influx of blood-derived cells, macromolecules and fluid. This ultimately leads to destructive cytotoxicity and vascular-origin edema, as well as life-threatening hemorrhagic transformation (3-5). In contrast to patients with mild BBB injury, patients with severe BBB injury exhibit higher National Institutes of Health Stroke Scale scores, worse functional outcomes and a greater risk of mortality (6,7). Therefore, alleviating the BBB injury can improve the neurological prognosis of patients with stroke (8).

Ferroptosis was initially reported in 2012 as a new form of regulated cell death that is distinct from apoptosis during the

processes of tumor and embryonic development (9). Research has indicated that ferroptosis is associated with BBB injury caused by CIRI (10). In 2017, research demonstrated that the inhibition of ferroptosis in a middle cerebral artery occlusion (MCAO) model protected mice from CIRI (11). Furthermore, dietary iron supplementation can enhance the rebuilding of the BBB and defend neurons following ischemic stroke (12,13). In addition, co-injection of ceruloplasmin and Fe^{2+} has been shown to significantly reduce BBB permeability, DNA damage, neuronal cell death and the degree of neurological deficits (14).

p23 is a protein with a molecular weight of 23 kDa, which is widely expressed in the heart, brain, kidney, lung and other tissues (15). Structural studies have reported that the N-terminus of the p23 protein contains a β-sheet domain consisting of two inverted β-sheets, and its C-terminus is an unfolded tail (16,17). Furthermore, yeast p23 has been reported to regulate the normal function of the Golgi apparatus, ribosome synthesis and DNA repair (18). Deletion of the p23 gene can lead to abnormal skin and lung tissue development, and perinatal death in mouse embryos (19). Several studies have shown that p23 can bind to a variety of proteins and serve a regulatory role in various diseases by regulating the biological functions of these target proteins. For example, the helical motif at the C-terminus of p23 can bind to the glucocorticoid receptor, thereby regulating its activity (20). In gastric cancer, p23 bound to gedunin is more efficiently cleaved by activated caspase 7, thereby promoting tumor cell apoptosis (21). However, to the best of our knowledge, the biological significance of p23 in ferroptosis caused by CIRI-induced BBB injury has not yet been studied.

The present study aimed to determine whether ferroptosis occurs in BMECs during ischemic stroke, and to investigate the regulation of p23 on BBB function and ferroptosis in BMECs during ischemic stroke, so as to explore its specific mechanism.

Materials and methods

Animals and ethics approval. Male Sprague-Dawley rats were acquired from the Experimental Animal Center of Central South University (Changsha, China). GPX4 $Fos^{CreERT2}$ mice (GPX4 $Fos^{CreERT2/-}$ and GPX4 $Fos^{CreERT2/+}$, GPX4 $Fos^{CreERT2/-}$ mice were used as controls for GPX4 $Fos^{CreERT2/+}$ mice to rule out the influence of the Cre recombinase or other experimental factors) were produced using GPX4-flox mice and $Fos^{CreERT2}$ mice (both obtained from GemPharmatech Co., Ltd.). It was confirmed that the expression levels of GPX4 were reduced in the brain tissues of GPX4 $Fos^{CreERT2/+}$ mice (Fig. S1). The rats that were aged 8 weeks and weighed 280±20 g underwent Ferrostatin-1 (Fer-1) or short hairpin (sh)RNA treatments, whereas the rats that were aged 6 weeks and weighed 130-150 g were treated with for adeno-associated virus. The mice were aged 8-12 weeks and weighed 22±25 g. All animals were kept in a room with a controlled temperature of 25˚C and humidity at 40-60% under a 12-h light/dark cycle, with free access to food and water.

A total of 78 rats and 30 GPX4 $Fos^{CreERT2}$ mice were used in the present study. For the Evans Blue extravasation test *in vivo*, 3 rats were allocated to the sham group, and 6 rats were allocated to the I/R 12-h group and the I/R 24-h group. For the ZO-1 and p23 immunofluorescence assay *in vivo*, 3 rats were allocated to the sham group and 6 rats were allocated to the I/R 12-h group. To assess the effects of Fer-1 on ZO-1 expression *in vivo*, 3 rats were allocated to the sham + vehicle group and the sham + Fer-1 group, whereas 6 rats were allocated to the I/R + vehicle group and I/R + Fer-1 group. For the p23 shRNA test *in vivo*, the sham + shNC group and sham + p23 shRNA group were each allocated 3 rats, and the I/R + shNC group and I/R + p23 shRNA group were each allocated 6 rats. For the p23 overexpression (OE) test *in vivo*, the sham + vector group and sham + OE p23 group were each allocated 3 rats, and the I/R + vector group and I/R + OE p23 group were each allocated 6 rats. For the GPX4 $Fos^{CreERT2}$ immunofluorescence assay *in vivo*, 3 GPX4 $Fos^{CreERT2/-}$ and 3 GPX4 $Fos^{CreERT2/+}$ mice were allocated to the sham + OE-vector group, and the I/R + OE-vector group and I/R + OE-p23 group were each allocated 6 GPX4 $Fos^{CreERT2/-}$ mice and 6 GPX4 $Fos^{CreERT2/+}$ mice. All experiments and animal procedures were approved by the Experimental Animal Center of Central South University (approval no. 2018sydw0222).

Cell culture and treatment. The mouse BMEC line bEnd.3 was procured from The Cell Bank of Type Culture Collection of The Chinese Academy of Sciences. The cells were cultured in DMEM (Gibco; Thermo Fisher Scientific, Inc.) supplemented with 10% FBS (Gibco; Thermo Fisher Scientific, Inc.) and 1% penicillin-streptomycin (Gen-View Scientific, Inc.) at 37˚C and 5% CO_2. bEnd.3 cells were used to establish an *in vitro* model of the BBB, and the oxygen-glucose deprivation/reoxygenation (OGD/R) experiment was used to simulate I/R injury *in vitro*. As for the administration of Fer-1 (Sigma-Aldrich; Merck KGaA), bEnd.3 cells were exposed to 10 μM Fer-1 at 37˚C for 2 h before OGD/R. For the cycloheximide (CHX) chase assay, CHX (10 μM; cat. no. NSC-185; Selleck Chemicals) was applied in OGD/R-insulted b.End 3 cells for 3-12 h at 37˚C to inhibit the proteasome pathway for the degradation of TJ proteins. The GPX4 agonist PKUMDL-LC-101-D04 (200 μM; CAS no. 2143896-83-5; MedChemExpress) was used to treat the cells for 1 h at 37˚C after OGD/R and p23 siRNA transfection, whereas the GPX4 inhibitor RAS-selective lethal 3 (RSL3; 200 nM; CAS no. 1219810-16-8; MedChemExpress) was used to treat the cells for 16 h at 37˚C after OGD/R and p23 oe.

Small interfering RNA (siRNA) transfection. siRNA transfection was performed using the riboFECT™ CP Transfection Kit (Guangzhou RiboBio Co., Ltd.) according to the manufacturer's instructions. Briefly, $1x10^6$ cells/well were plated in 6-well plates and cultured for 12-24 h until the cell density reached 50-60%. The transfection complex was prepared by diluting 5 μl 20 μM siRNA storage solution with 120 μl 1X riboFECT CP Buffer, adding 12 μl riboFECT CP Reagent and incubating at room temperature for 15 min. The transfection complex was then added to the medium and cultured in a CO_2 incubator at 37˚C for 24 h. A negative control (NC) siRNA that does not target any known human, mouse or rat genes, and is not chemically modified, was used as a NC (cat. no. siN0000001-1-10; Guangzhou RiboBio Co., Ltd.). The of p23 siRNA sequence was as follows: 5'-GGTCCTGTTTGAACAAAGA-3'. The cell

Table I. p23 truncated sequences.

Truncation	Sequence, 5'-3'
p23(1-160)	ATGGACTACAAGGATGACGATGACAAGGATTACAAAGACGACGATGATAAGGACTATAAGGATGA TGACGACAAAATGCAGCCTGCTTCTGCAAAGTGGTACGATCGAAGGGACTATGTATTCATTGAATT TTGTGTTGAAGACAGTAAAGATGTTAATGTAAACTTTGAAAAATCCAAACTTACTTTCAGTTGTCT TGGAGGAAGCGATAATTTTAAGCATTTAAATGAAATTGATCTTTTTCATTGTATCGATCCAAATGATT CCAAGCATAAAAGAACAGACAGATCGATTTTATGTTGTTTGCGAAAAGGAGAATCCGGCCAGTCA TGGCCTAGGTTAACAAAGGAAAGGGCAAAGCTTAATTGGCTCAGTGTGGACTTCAATAATTGGAA AGACTGGGAGGATGACTCAGATGAAGACATGTCGAATTTTGACCGTTTCTCTGAGATGATGGATCA CATGGGTGGTGATGAGGATGTAGATTTACCAGAAGTAGATGGAGCAGATGATGATTCACAAGACA GTGATGATGAAAAGATGCCAGATCTGGAGTAA
p23(1-90)	ATGGACTACAAGGATGACGATGACAAGGATTACAAAGACGACGATGATAAGGACTATAAGGATGA TGACGACAAAATGCAGCCTGCTTCTGCAAAGTGGTACGATCGAAGGGACTATGTATTCATTGAATT TTGTGTTGAAGACAGTAAAGATGTTAATGTAAACTTTGAAAAATCCAAACTTACTTTCAGTTGTCT TGGAGGAAGCGATAATTTTAAGCATTTAAATGAAATTGATCTTTTTCATTGTATCGATCCAAATGAT TCCAAGCATAAAAGAACAGACAGATCGATTTTATGTTGTTTGCGAAAAGGAGAATCCGGCCAGTC ATGGCCTAGGTTAACATAA
p23(91-160)	ATGGACTACAAGGATGACGATGACAAGGATTACAAAGACGACGATGATAAGGACTATAAGGATGAT GACGACAAAAAGGAAAGGGCAAAGCTTAATTGGCTCAGTGTGGACTTCAATAATTGGAAAGACTG GGAGGATGACTCAGATGAAGACATGTCGAATTTTGACCGTTTCTCTGAGATGATGGATCACATGGG TGGTGATGAGGATGTAGATTTACCAGAAGTAGATGGAGCAGATGATGATTCACAAGACAGTGATGA TGAAAAGATGCCAGATCTGGAGTAA

samples were subjected to OGD. After 3 h of OGD exposure, the cells were cultured in normal medium containing 10% FBS within a cell incubator containing 5% CO_2 at 37˚C for 12 h.

Plasmid transfection. The p23 OE plasmid, truncated p23 plasmids and blank vector plasmid (GV486; both from Shanghai GeneChem Co., Ltd.) were transfected into cells using the Neofect™ DNA transfection reagent (Neofect Biotech Co., Ltd.) according to the manufacturer's protocol. The truncated p23 sequences are provided in Table I. A total of $1x10^6$ cells/well were plated in 6-well plates and cultured for 12-24 h until they reached a cell density of 60-80%. The DNA diluent was prepared by adding 100 μl Opti-MEM serum-free (Gibco; Thermo Fisher Scientific, Inc.) to 2 μg plasmid. Subsequently, 2 μl Neofect was added to the DNA diluent and incubated at room temperature for 15-30 min. Finally, the complex was added to the cells in 6-well plates and cultured in a CO_2 incubator at 37˚C for 48 h.

Cell viability assay. Cell viability was assessed using the Cell Counting Kit-8 (CCK-8; cat. no. GK3607; Gen-View Scientific, Inc.). A total of 5,000 cells were seeded in a 96-well plate and were cultured for ~24 h. Following treatment, CCK-8 was added to the medium in each well at a 1:10 ratio and the cells were incubated at 37˚C for 1-4 h. Subsequently, the colorimetric absorbance of each well was measured at 450 nm using a microplate reader and a ratio was calculated compared with the control group.

Reverse-transcription quantitative PCR (RT-qPCR). Following extraction with TRIzol® reagent (Invitrogen; Thermo Fisher Scientific, Inc.), 1 μg RNA from cells or animal brain samples was reverse transcribed using 5X Evo M-MLV RT Reaction Mix (Accurate Biology) according to the manufacturer's protocol. Subsequently, qPCR was carried out according to the manufacturer's protocol using the SYBR Premix Ex Taq II kit (Accurate Biology) with the following amplification conditions: Pre-denaturation at 95˚C for 30 sec, followed by 40 cycles at 95˚C for 5 sec and 60˚C for 34 sec. The primer sequences used are presented in Table II. The relative quantification of mRNA was analyzed using the $2^{-\Delta\Delta Cq}$ method (22).

Western blotting. Proteins from cells or animal brain samples were extracted using radioimmunoprecipitation assay lysis buffer (Guangzhou Dingguo Biotechnology Co., Ltd.) containing 1% PMSF, and were quantified using the BCA method. Subsequently, 20-30 μg cell proteins or 50-80 μg animal proteins were transferred to a PVDF membrane following SDS-PAGE on 10-15% gels. Subsequently, the membranes were blocked with TBS-1% Tween 20 (TBST) containing 5% skim milk powder at room temperature for 2 h. The membranes were then incubated with primary antibodies against β-actin (cat. no. A1978; dilution, 1:5,000; Sigma-Aldrich; Merck KGaA), p23 (cat. no. 160150; dilution 1:200; Cayman Chemical Company), zonula occludens-1 (ZO-1; cat. no. 402200; dilution 1:2,000; Invitrogen; Thermo Fisher Scientific, Inc.), occludin (cat. no. 404700; dilution 1:1,000; Invitrogen; Thermo Fisher Scientific, Inc.), GPX4 (cat. no. ab125066; dilution 1:3,000; Abcam), cyclooxygenase (COX)-2 (cat. no. 160106; dilution 1:200; Cayman Chemical Company), heat shock protein 90 (HSP90; cat. no. 60318-1-lg;

Table II. Primer sequences used in the present study.

Primer	Forward sequence, 5'-3'	Reverse sequence, 5'-3'
GPX4	ATAAGAACGGCTGCGTGGTGAAG	TAGAGATAGCACGGCAGGTCCTTC
ZO-1	CTGGTGAAGTCTCGGAAAAATG	CATCTCTTGCTGCCAAACTATC
Occludin	TGCTTCATCGCTTCCTTAGTAA	GGGTTCACTCCCATTATGTACA
p23	AGGAAAGGGCAAAGCTTAATTG	TCATCTCAGAGAAACGGTCAAA
COX-2	ATTCCAAACCAGCAGACTCATA	CTTGAGTTTGAAGTGGTAACCG
β-actin	CTACCTCATGAAGATCCTGACC	CACAGCTTCTCTTTGATGTCAC

COX-2, cyclooxygenase-2; GPX4, glutathione peroxidase 4; ZO-1, zonula occludens-1.

dilution 1:2,000; Proteintech Group, Inc.) and Flag (cat. no. 20543-1-AP; dilution 1:2,000; Proteintech Group, Inc.) at 4˚C overnight. The membranes were washed with TBST three times at 10-min intervals and were then incubated with the HRP-conjugated goat anti-rabbit IgG (cat. no. BA1055; dilution 1:5,000; Boster Biological Technology) or goat anti-mouse IgG (cat. no. BA1056; dilution 1:5,000; Boster Biological Technology) secondary antibodies at room temperature for 1 h, followed by three further washes with TBST at 10-min intervals. The color reaction was developed using the Clarity Western ECL Substrate (cat. no. 170-5061; Bio-Rad Laboratories, Inc.), and band density was measured using ImageJ software V 1.8.0 (National Institutes of Health) and was normalized to β-actin.

Immunofluorescence. After fixing with 4% paraformaldehyde for 10 min at room temperature, 5,000 bEnd.3 cells grown in 96-well plates were washed three times with PBS (5 min each) and were blocked with BSA (Gen-View Scientific, Inc.) at 37˚C for 1 h. The cells were then incubated with a primary antibody against ZO-1 (cat. no. 61-7300; dilution 1:50; Invitrogen; Thermo Fisher Scientific, Inc.), p23 (dilution 1:20; cat. no. 160150; Cayman Chemical Company), CD31 (cat. no. ab9498; dilution 1:1,000; Abcam) and GPX4 (dilution 1:100; cat. no. ab125066; Abcam) at 4˚C overnight. The cells were then incubated with a TRITC-conjugatedsecondary antibody (cat. no. AS040; dilution 1:1,000; ABclonal Biotech Co., Ltd.) at 37˚C in the dark for 1 h. Nuclei were stained with 1X DAPI working solution at room temperature for 5 min, washed three times with PBS-1% Tween 80 (PBST) and images were captured using a fluorescence microscope (Olympus Corporation).

Experimental MCAO model. The rats or GPX4 $Fos^{CreERT2}$ mice were anaesthetized through an intraperitoneal injection of 50 mg/kg sodium pentobarbital (China National Pharmaceutical Group). An incision was made in the neck to expose the external carotid, internal carotid, right common carotid and common carotid arteries, and the internal carotid artery was clamped. Following the ligation of the external carotid artery, a small incision was made into the external carotid artery. Monofilaments coated with poly-L-lysine were inserted via the incision, through the internal carotid artery and ultimately to the middle cerebral artery. Following occlusion (2 h for rats and 1 h for mice), the nylon monofilament was withdrawn for reperfusion for 24 h. The sham group underwent the same procedure as the MCAO group without insertion of the monofilament. The survival and health status of the animals was observed every 3 h. The cortex of the infarcted hemisphere was collected for subsequent experiments at 12 or 24 h post-reperfusion. The animals were euthanized by rapid dislocation of the head and neck when it was time to collect the specimens, or when the animals reached the following humane endpoints: They were too weak to eat or drink for up to 24 h; they were in a moribund state, i.e., without anesthesia or sedation, they were showing mental depression accompanied by hypothermia (<37˚C). The loss of respiratory movement (the rise and fall of the chest and abdomen), and reflex actions of the eyes, nose and feet were used to verify the death of the animals. Notably, after MCAO treatment, 12 rats and 8 mice were sacrificed before sample collection, and 6 rats and 4 mice died spontaneously.

Lateral ventricle injection. After anesthetizing with 50 mg/kg sodium pentobarbital and preserving the skin on the top of the head, the rats were positioned horizontally and prone on a stereotaxic frame (RWD Life Science). Subsequently, 40 nmol/kg Fer-1, with saline used as a vehicle control; or p23 shRNA [forward (5'-3'): CCGGGATCCTAGACCATG GATTTAACT CGAGTTAAATCCATGGTCTAGGATCTT TTTG, reverse (5'-3'): AATTCAAAAAGATCCTAGACC ATGGATTTAACTCGAGTTAAATCCATGGTCTAGGATC; pRNAT-U6.1/Neo, Guangzhou RiboBio Co., Ltd.], with shNC [forward (5'-3'): TACGATACAAGGCTGTTAGAG AG, reverse (5'-3'): TAGAAGGCACAGTCGAGG used as the control] was infused into the right lateral ventricle at a flow rate of 0.5 μl/min using a syringe pump (KD Scientific) in conjunction with a Hamilton syringe. The stereotaxic coordinates for the right lateral ventricle were -1.5 mm laterally, -1.2 mm anteroposteriorly and -4.5 mm dorsoventrally, with the bregma point serving as the origin. The p23 OE adeno-associated virus (AAV-9; Shanghai GeneChem Co., Ltd.) was injected into the right lateral ventricle -1.2 mm laterally, -0.8 mm anteroposteriorly and -3.5 mm dorsoventrally, with empty AAV-9 used as the vector control. Following the injection, the skull was sealed using bone wax. OE was induced 2-3 weeks after injection. Similarly, the lateral ventricle injection of GPX4 $Fos^{CreERT2}$ mice was performed as that performed in rats; the stereotaxic coordinates were as follows: -1.2 mm laterally, -0.8 mm anteroposteriorly and -3.5 mm dorsoventrally. Subsequently,

the animals underwent MCAO modeling and the brain tissue was collected for testing.

In vivo BBB permeability assay. In rats, the permeability of the BBB was evaluated through Evans Blue extravasation. A 2% Evans Blue solution was prepared using normal saline prior to the experiment. A total of 1 h before the conclusion of reperfusion, 2% Evans Blue (2 ml/kg) was injected into the tail vein of the rats. After 1 h, the rats were anesthetized with 50 mg/kg sodium pentobarbital and underwent cardiac perfusion with PBS. The brains were then collected and 2-mm thick coronal sections were made.

OGD/R. Cells were subjected to a 3-h culture in glucose- and serum-free medium in an anaerobic incubator (37˚C, 95% N_2, 5% CO_2). After 3 h of OGD exposure, the cells were cultured in normal medium containing 10% FBS within a cell incubator containing 5% CO_2 at 37˚C for 12 and 24 h. The control group cells were cultured under normoxic condition, while the 0 h OGD/R group underwent OGD without reperfusion. The cell samples were then collected for subsequent experiments.

In vitro permeability assay. The bEnd.3 cells were cultured on the upper chamber of gelatin-coated Transwell inserts (0.4 μm; Costar; Corning, Inc.) and were exposed to hypoxic conditions (0% O_2) at 37˚C for 3 h. Subsequently, 165 μg/ml Evans Blue -0.1% BSA (Sigma Aldrich; Merck KGaA) was added to the upper chamber 1 h prior to measurements. The intensities of the diffused Evans Blue -0.1% BSA in the lower chamber were subsequently measured at 650 nm using a microplate reader. The results are presented as the ratio of the Evans Blue -0.1% BSA concentration in the lower chamber to the total concentration of Evans Blue -0.1% BSA added to the upper chamber at the onset of the experiment.

Reactive oxygen species (ROS) assay. Using the fluorescent probe diacetyldichlorofluorescein (DCFH-DA) ROS detection kit (cat. no. S0033S; Beyotime Institute of Biotechnology), DCFH-DA was diluted at a ratio of 1:1,000 with serum-free medium to a final concentration of 10 μM. Subsequently, the cell culture medium was removed from the cells, an appropriate volume of diluted DCFH-DA was added and incubation was carried out in a cell incubator at 37˚C for 20 min. The cells were then washed with PBS three times, and a 488-nm excitation wavelength and 525-nm emission wavelength were used to detect the optical density using a microplate reader.

Malondialdehyde (MDA) assay. The MDA assay was conducted using a Lipid Peroxidation MDA Assay Kit (cat. no. S0131S; Beyotime Institute of Biotechnology). Following homogenization, the brain or cell samples were centrifuged at 13,000 x g and 4˚C for 10 min to obtain the supernatant for detection. Subsequently, the prepared thiobarbituric acid working solution was added and heated at 100˚C for 15 min. Eventually, the mixtures were centrifuged at 13,000 x g and 4˚C for 10 min to obtain the supernatant, which was transferred to a 96-well plate to measure absorbance at 532 nm using a microplate reader. The content of MDA was normalized with respect to the protein amount of the samples, which was determined using the BCA method.

Glutathione (GSH) assay. The GSH assay was conducted using a GSH and reduced glutathione (GSSG) assay kit (cat. no. S0053; Beyotime Institute of Biotechnology) according to the manufacturer's protocol. After OGD/R treatment, the cells were collected and resuspended with protein removal agent M. After rupturing the cell membrane through two freeze-thaw cycles, the cells were centrifuged at 10,000 x g at 4˚C for 10 min and the supernatant was used for the determination of total GSH. Part of the supernatant was taken for GSSG detection: GSH removal auxiliary solution and GSH removal reagent working solution were added, and the reaction was performed at 25˚C for 60 min. The protein removal reagent M solution and total GSH detection working solution were then added to the samples for total GSH or GSSG detection, and were incubated at 25˚C for 5 min, before the addition of NADPH. The absorbance of the sample was detected at 512 nm with a microplate reader. The GSH content was calculated as follows: GSH=total GSH-GSSG x2. The GSH content was normalized with respect to the protein amount of the samples, which was determined using the BCA method.

Molecular docking. The structures of HSP90, p23 and GPX4 were downloaded from the Protein Data Bank (PDB) database (https://www.rcsb.org/); HSP90 and p23 are in the same protein file (PDB ID: 7L7J), whereasGPX4 (PDB ID: 6HN3) has its own protein structure file. The interaction modes between GPX4, HSP90 and p23 were investigated using the ZDOCK (https://zdock.wenglab.org/) server.

Transmission electron microscopy. Briefly, 5,000 cells/well were plated on a 96-well slide. After OGD/R, the cells were washed with PBS and successively fixed with 2.5% glutaraldehyde and 1% osmium acid at room temperature for 6 h. Following dehydration using varying concentrations of acetone, the samples were embedded in acetone and embedding solution at room temperature for 12 h, and solidified in an oven at 60˚C for 24 h. Subsequently, the slides were double-stained with 3% uranium acetate and lead nitrate at room temperature for 2-3 min. Finally, the samples were observed and images were captured using a Hitachi HT7700 transmission electron microscope (Hitachi, Ltd.).

Co-immunoprecipitation assay. This assay was performed using agarose beads (Thermo Fisher Scientific, Inc.). Proteins from cell samples were extracted using radioimmunoprecipitation assay lysis buffer (Guangzhou Dingguo Biotechnology Co., Ltd.). After extraction, 300 μg cellular protein was incubated with the p23 (cat. no. 160150; dilution 1:200; Cayman Chemical Company), GPX4 (cat. no. ab125066; dilution 1:3,000; Abcam), and Flag (cat. no. 20543-1-AP; dilution 1:2,000; Proteintech Group, Inc.) antibodies at 4˚C for 1 h with agitation. Subsequently, 20 μl suspended agarose beads were added and incubated at 4˚C overnight with agitation. The immunoprecipitation products were collected and centrifuged at 2,500 x g for 5 min at 4˚C, and the supernatant was discarded. The agarose beads were washed with PBST and centrifuged again; this was repeated four times. Finally, the agarose beads were resuspended with 40 μl electrophoretic loading buffer, boiled at 85˚C for 5 min, and 20 μl samples underwent SDS-PAGE and western blotting.

Statistical analysis. All experiments were independently repeated at least three times. The results, presented as the mean ± SD, were analyzed using one-way or two-way ANOVA along with the multiple-comparison Bonferroni correction test. Statistical analysis was performed using GraphPad Prism 8 software (GraphPad Software Inc.). $P<0.05$ was considered to indicate a statistically significant difference.

Results

Increased permeability of BMECs in ischemic stroke. To investigate the effect of the MCAO model on BBB dysfunction, the Evans Blue extravasation test was used to measure cerebral microvascular permeability. As shown in Fig. 1A, the ischemia group had markedly higher Evans Blue leakage than the sham group. TJ proteins are transmembrane proteins located between endothelial cells of the BBB, which serve critical roles in regulating the paracellular permeability of the BBB (23). The TJ protein ZO-1 was markedly decreased after 12-h I/R (Fig. 1B). To investigate the effects of OGD/R on BBB permeability during hypoxia *in vitro*, a Transwell assay was used to generate an *in vitro* BBB model, and BBB permeability was measured in BMECs using Evans Blue staining. The content of Evans Blue in the lower Transwell chamber was higher in the 0 and 12 h OGD/R groups than in the normoxia group (Fig. 1C). Subsequently, western blotting was performed to determine whether OGD/R affected the protein levels of ZO-1 and occludin. The expression levels of ZO-1 and occludin were decreased in BMECs in the OGD/R group at 12 h after reoxygenation compared with those in the control group (Fig. 1D-F). In addition, the expression of the TJ ZO-1 was detected in OGD/R-treated BMECs using immunofluorescence. The results showed that the expression of ZO-1 in BMECs in the OGD/R group was significantly decreased and exhibited a discontinuous distribution (Fig. 1I and J).

Ferroptosis in BMECs is involved in BBB damage in ischemic stroke. Increasing evidence has indicated that ferroptosis in BMECs is the main cause of BBB injury induced by I/R (24,25). Pretreatment with Fer-1 was performed via intraventricular injection for 2 h, followed by MCAO modeling, and the results showed that, as compared with in the sham + vehicle (saline) group, ZO-1 expression in brain tissues was decreased in the I/R + vehicle group, whereas it was increased in the I/R + Fer-1 group compared with that in the I/R + vehicle group (Fig. 2A). In addition, BMECs were pretreated with Fer-1, and it was revealed that the reduction in cell viability induced by OGD/R was significantly suppressed (Fig. 2B). Following OGD/R, BMECs exhibited mitochondrial swelling, and a decrease or disappearance in cristae (Fig. 2C), as well as decreased levels of the antioxidant molecules GSH and GPX4, and increased levels of MDA and ROS (Fig. 2D-J). This indicated that intracellular lipid peroxidation levels were increased. In addition, the expression levels of COX-2, another biomarker of ferroptosis, were significantly increased in the 12 h OGD/R group (Fig. 2K-M). These results suggested that ferroptosis may be involved in OGD/R-induced BMECs injury. Inhibiting ferroptosis in BMECs could protect against BBB damage caused by cerebral I/R.

p23 protects against BMEC injury in ischemic stroke. p23 can bind to client proteins and serves a regulatory role in numerous diseases by regulating their biological functions. In the present study, the *in vitro* results showed that p23 expression was significantly induced by OGD/R in BMECs (Fig. 1D, G and H) Subsequently, the permeability of BMECs was examined following OE or knockdown of p23 in BMECs. First, in the OGD/R model, siRNA was used to knockdown p23 expression (Fig. 3A), the results showed that p23 and ZO-1 expression levels were inhibited by p23 knockdown (Fig. 3C and D), and the permeability of BMECs was clearly increased (Fig. 3B), which indicated that the injury of BMECs induced by OGD/R was aggravated by p23 knockdown. Transfection with the p23 OE plasmid significantly increased the expression of p23 in the OGD/R model (Fig. 4A-C). Compared with in the vector + OGD/R group, the content of Evans Blue in the p23 + OGD/R group was significantly decreased (Fig. 4D and E), and the expression of ZO-1 was increased (Fig. 4F), which indicated that the OE of p23 reversed the OGD/R-induced damage of BMECs. *In vivo*, p23 knockdown by shRNA reduced the expression of ZO-1 in the MCAO group compared with that in the MCAO + shNC group (Fig. 3E), while p23 OE in the MCAO group could rescue the decrease in ZO-1 compared with in the MCAO + vector group (Fig. 4G); CD31 was used to indicate the location of blood vessels.

p23 protects against OGD/R-induced ferroptosis in BMECs. Given that ferroptosis is involved in BBB damage in ischemic stroke, the effect of p23 on OGD/R-induced ferroptosis in BMECs was determined. Compared with in the control group, the mortality of BMECs increased by p23 knockdown (Fig. 5A). In addition, p23 was overexpressed at the cellular level, and p23 could rescue cell death induced by OGD/R (Fig. 5B). In the OGD/R group, transfection with the p23 siRNA further decreased the contents of GSH and GPX4, and increased the levels of ROS, MDA, and acyl-CoA synthetase long-chain family member 4 (ACSL4) and subunit solute carrier family 7 member 11 (SLC7A11; Fig. 5C-I) compared with in the OGD/R + NC group, indicating that the increase of lipid peroxidation in BMECs promoted OGD/R-induced ferroptosis. After OGD/R, p23 OE decreased the levels of ROS, MDA, ACSL4 and SLC7A11, and increased those of GSH and GPX4 compared with those in the vector group (Fig. 5J-P), indicating that the levels of antioxidants in BMECs were increased, inhibiting OGD/R-induced ferroptosis. These results suggested that the regulatory role of p23 in OGD/R-induced BMECs may be achieved through ferroptosis.

p23 enhances GPX4 stability to suppress ferroptosis. Notably, p23 can function as an independent molecular chaperone or as a co-chaperone of HSP90 to exert its biological functions (26). To further explore the mechanism of p23-induced inhibition of ferroptosis, protein docking showed that p23 formed a complex with HSP90 and GPX4 through its N-terminal domain (1-90aa) (Fig. 6A). Co-IP experiments demonstrated that anti-GPX4 antibodies could precipitate p23 and HSP90 proteins in cells. Similarly, anti-p23 antibodies could precipitate GPX4 and HSP90 proteins in cells. (Fig. 6B). Full-length and truncated p23 plasmids were then constructed: Flag-p23(1-160),

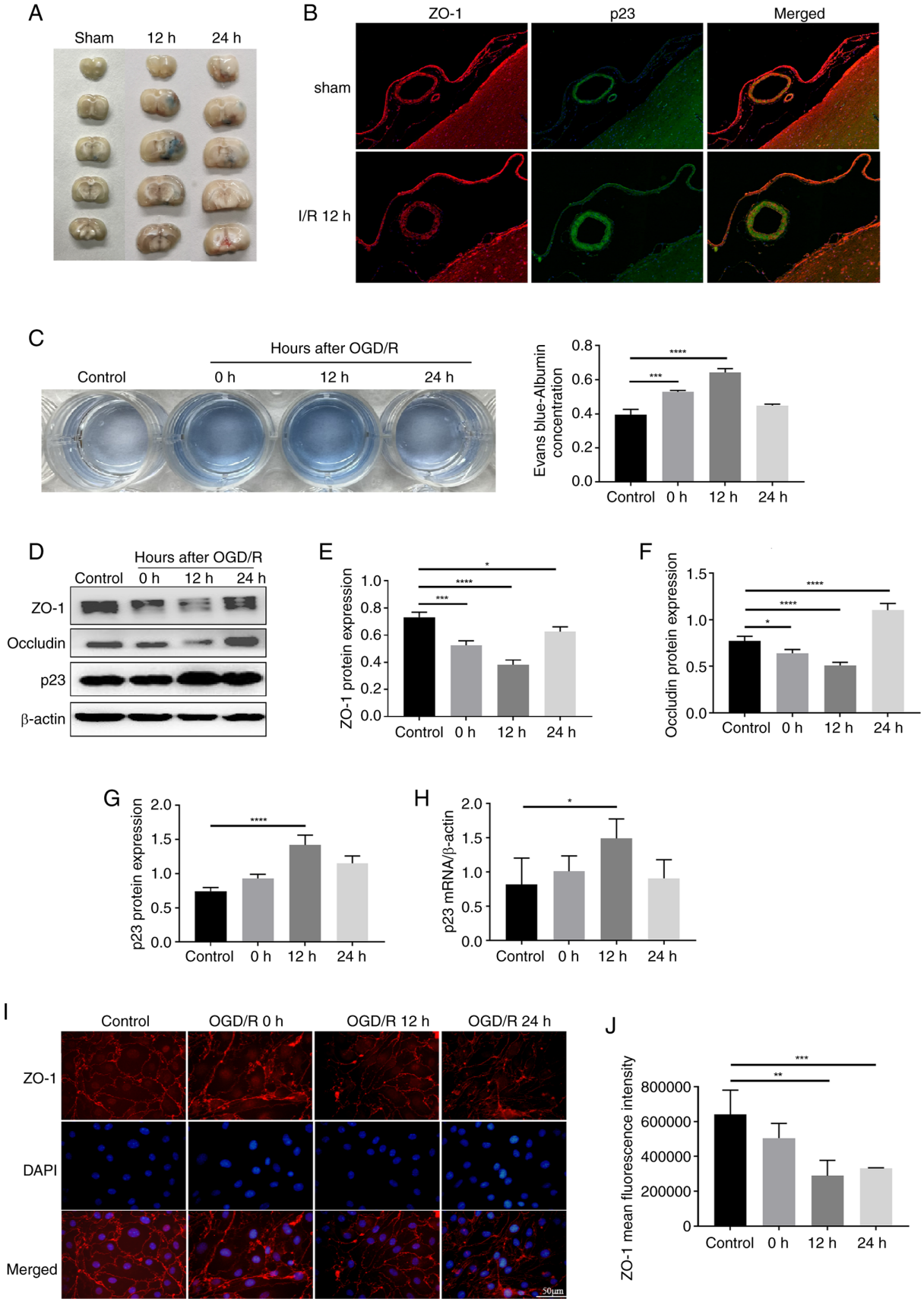

Figure 1. I/R-induced injury of BMECs. (A) Evans Blue extravasation test was used to measure BBB permeability in rats with different perfusion times. (B) Immunofluorescence showed colocalization of p23 (green) and ZO-1 (red). (C) A Transwell system was used to establish an *in vitro* BBB model, and the permeability of BMECs was measured using Evans Blue and underwent statistical analysis (n=3). (D) Protein expression levels of (E) ZO-1 (n=3), (F) occludin (n=3) and (G) p23 (n=3) were determined by western blotting in BMECs following OGD/R. (H) Expression of p23 in BMECs after OGD/R was detected by quantitative PCR (n=3). (I) Expression of ZO-1 in BMECs after OGD/R was detected by immunofluorescence and (J) statistical analysis was performed (n=3) (magnification, x200). Data are presented as the mean ± SD. *P<0.05, **P<0.01, ***P<0.001 and ****P<0.0001. I/R, ischemia/reperfusion; BMECs, brain microvascular endothelial cells; BBB, blood-brain barrier; ZO-1, zonula occludens-1; OGD/R, oxygen-glucose deprivation/reoxygenation.

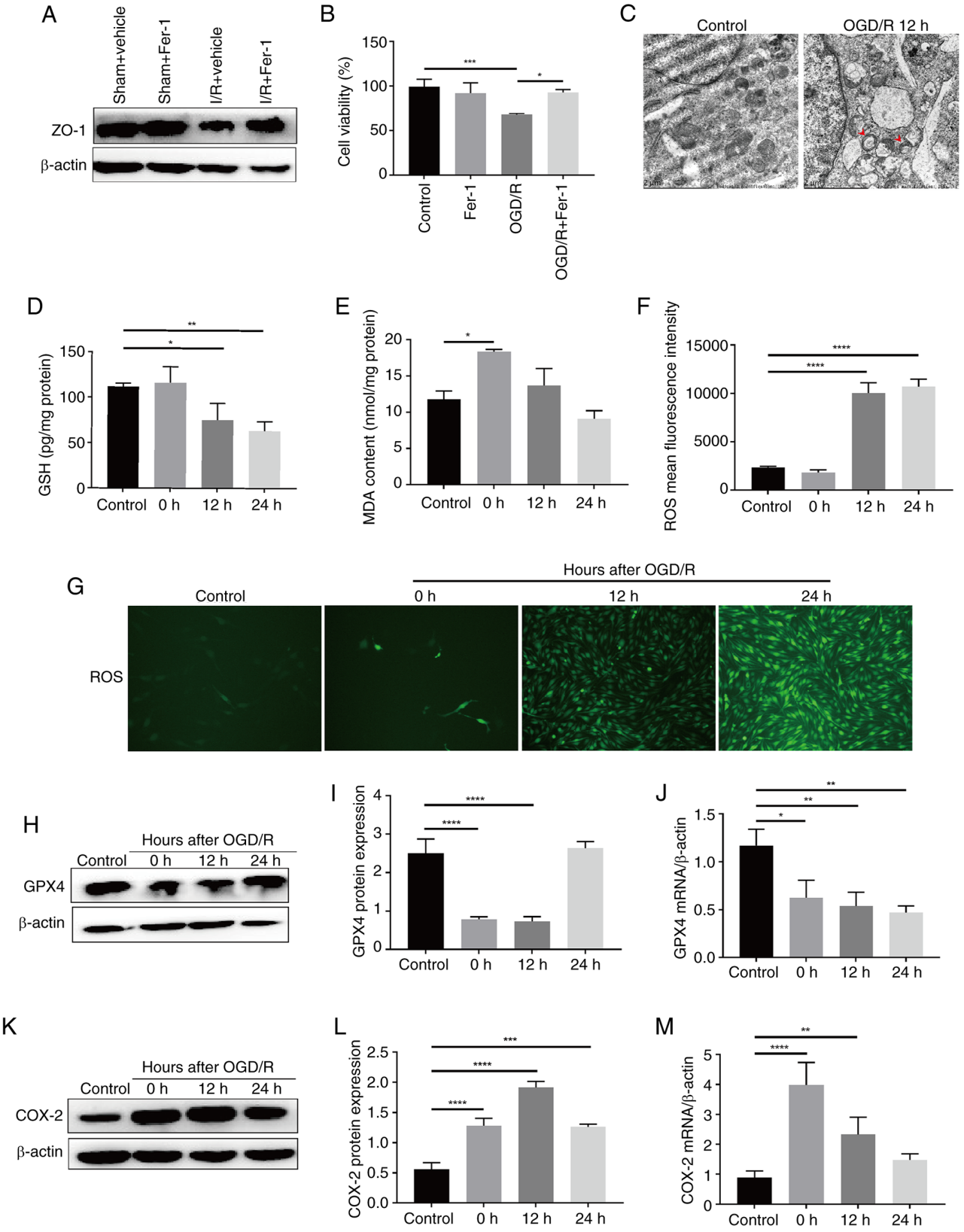

Figure 2. Ferroptosis is involved in OGD/R-induced BMEC injury. (A) Expression levels of ZO-1 protein in the rat brain tissue of a middle cerebral artery occlusion after 2 h of Fer-1 pretreatment were determined by western blotting. (B) Viability of BMECs induced by OGD/R following pretreatment with Fer-1 was determined using the Cell Counting Kit-8 assay (n=3). (C) Representative transmission electron microscopy images displaying the morphology of mitochondria in BMECs following OGD/R. The mitochondria presented increased membrane density and a shrunken form (indicated by red arrows) (magnification, x20,000). Intracellular (D) GSH (n=3), (E) MDA (n=3) and (F) ROS (n=3) levels in BMECs following OGD/R. (G) Representative images of intracellular ROS levels in BMECs following OGD/R (magnification, x100). (H) Protein expression levels and (I) statistical analysis (n=3), and (J) mRNA levels (n=3) of GPX4 in BMECs following OGD/R. (K) Protein expression levels and (L) statistical analysis (n=3), and (M) mRNA levels (n=3) of COX-2 in BMECs following OGD/R. Data are presented as the mean ± SD. *P<0.05, **P<0.01, ***P<0.001 and ****P<0.0001. OGD/R, oxygen-glucose deprivation/reoxygenation; BMECs, brain microvascular endothelial cells; ZO-1, zonula occludens-1; Fer-1, Ferrostatin-1; GSH, glutathione; GPX4, glutathione peroxidase 4; MDA, malondialdehyde; ROS, reactive oxygen species; COX-2, cyclooxygenase-2.

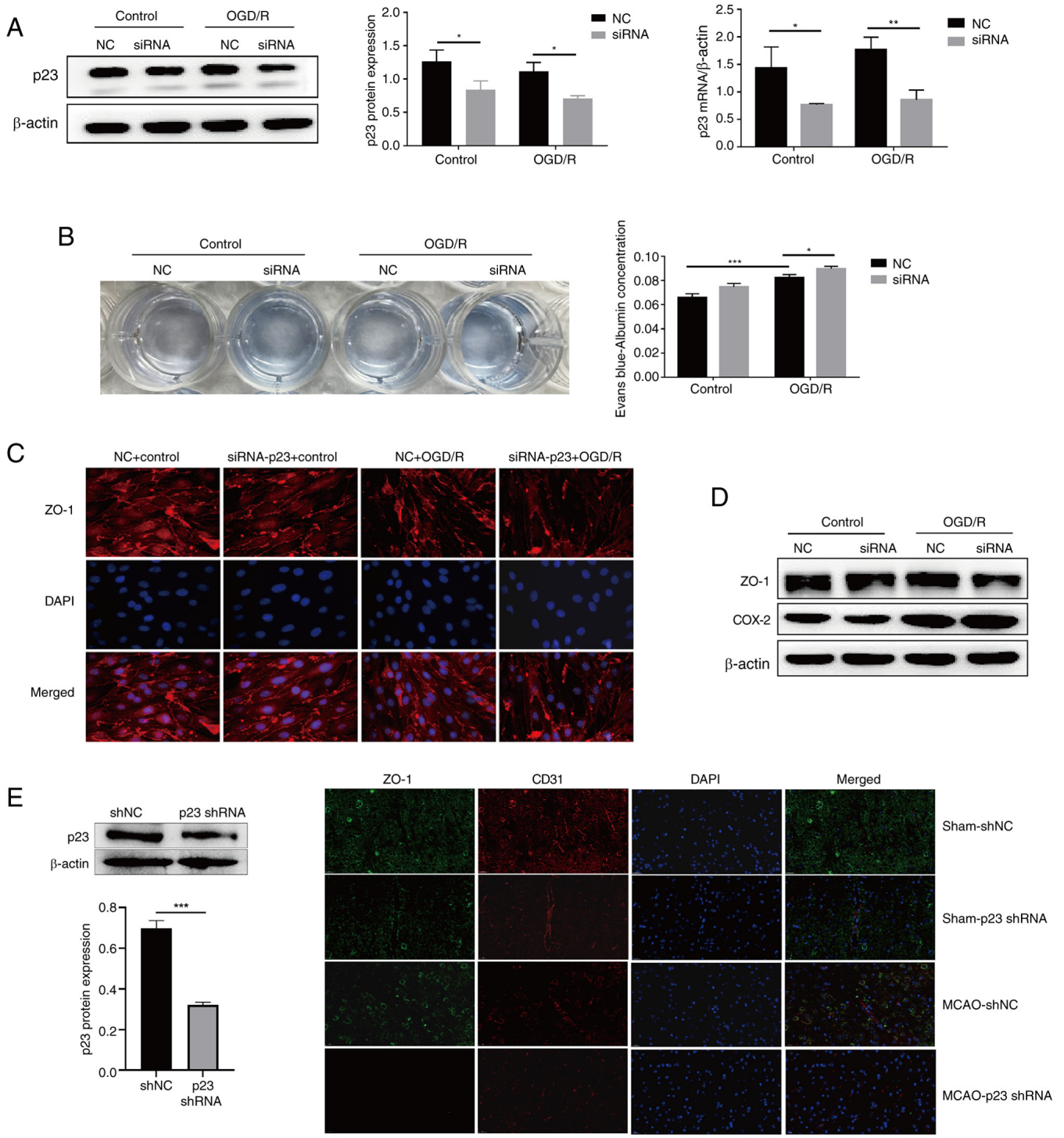

Figure 3. p23 protects against BMEC injury in ischemic stroke. (A) p23 expression levels in BMECs with p23 siRNA-mediated knockdown (n=3). (B) Permeability of BMECs induced by OGD/R following p23 siRNA transfection was detected using Evans Blue (n=3). (C) Expression of ZO-1 in BMECs induced by OGD/R following p23 siRNA transfection was detected using immunofluorescence (magnification, x200). (D) Expression of ZO-1 and COX-2 in rats following MCAO and p23 shRNA treatment was detected using western blotting. (E) Expression levels of p23 (western blot repeats, n=3) and ZO-1 (magnification, x100) were detected in rats following MCAO and p23 shRNA treatment. Data are presented as the mean ± SD. *P<0.05, **P<0.01 and ***P<0.001. BMECs, brain microvascular endothelial cells; siRNA, small interfering RNA; NC, negative control; sh, short hairpin; OGD/R, oxygen-glucose deprivation/reoxygenation; ZO-1, zonula occludens-1; COX-2, cyclooxygenase-2; MCAO, middle cerebral artery occlusion.

N-terminal Flag-p23(1-90) and C-terminal Flag-p23(91-160) fragments. After transfecting the BMECs with the truncated plasmids, immunoprecipitation was performed with anti-Flag antibody. The results showed that GPX4 could be precipitated by anti-Flag antibody, and the most important binding region was p23(1-90), which indicated that p23 formed a complex with HSP90 and GPX4 to inhibit GPX4 degradation and stabilize the expression of GPX4 through the N-terminal domain (1-90aa) of p23, thus inhibiting ferroptosis (Fig. 6C). In addition, immunofluorescence co-localization verification showed that p23 and GPX4 were co-located in cells (Fig. 6D). The effect of p23 on the stability of GPX4 protein was then

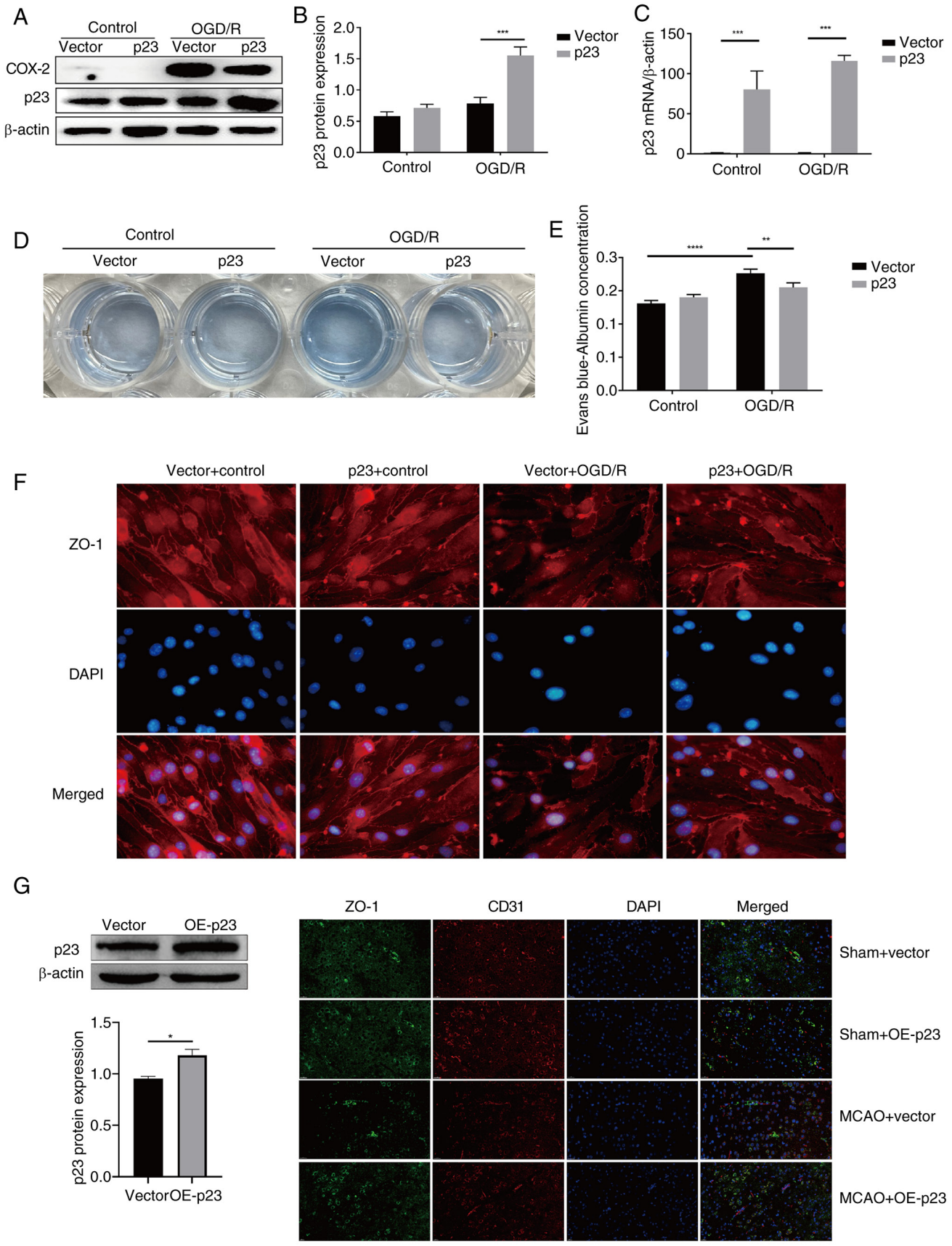

Figure 4. p23 protects against BMECs injury in ischemic stroke. (A) Western blot analysis of p23 and COX-2 expression levels in BMECs with p23 OE. Statistical analysis of (B) protein levels and (C) mRNA levels of p23 in BMECs with p23 OE (n=3). (D) Permeability of BMECs in an OGD/R model following p23 OE was detected using Evans Blue. (E) Statistical analysis of permeability of BMECs in an OGD/R model following p23 OE (n=3). (F) ZO-1 expression in BMECs in an OGD/R model following p23 overexpression was detected by immunofluorescence (magnification, x200). (G) p23 (western blot repeats, n=3) and ZO-1 (magnification, x100) expression were detected in rats following MCAO and p23 OE treatment. Data are presented as the mean ± SD. *P<0.05, **P<0.01, ***P<0.001 and ****P<0.0001. BMECs, brain microvascular endothelial cells; OGD/R, oxygen-glucose deprivation/reoxygenation; ZO-1, zonula occludens-1; MCAO, middle cerebral artery occlusion; OE, overexpression.

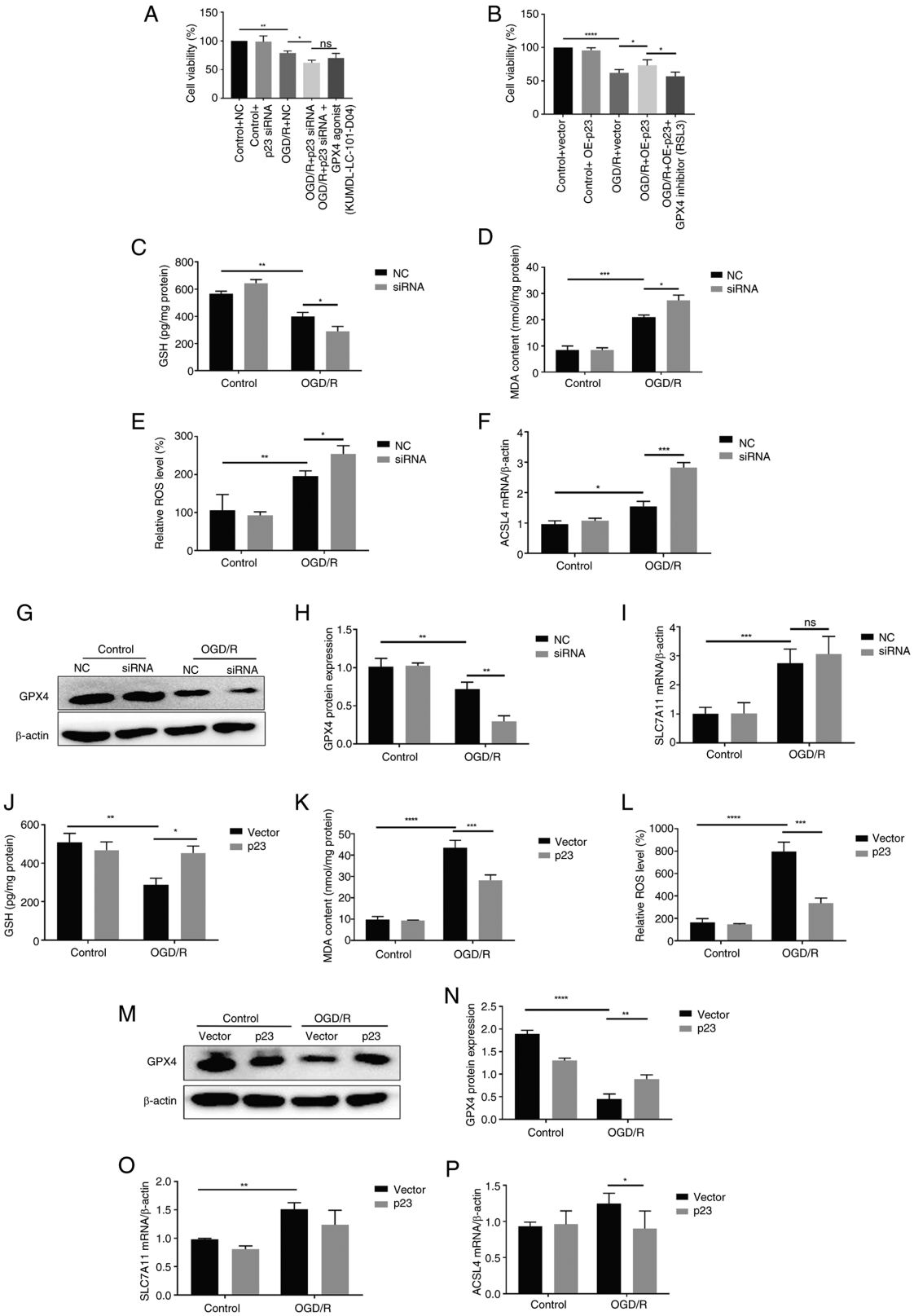

Figure 5. p23 protects against OGD/R-induced ferroptosis of BMECs. (A) Cell viability induced by OGD/R following transfection with p23 siRNA in BMECs was detected using the CCK-8 assay (n=3). (B) Cell viability induced by OGD/R following transfection with p23 OE vector in BMECs was detected using the CCK-8 assay (n=3). Intracellular (C) GSH (n=3), (D) MDA (n=3) and (E) ROS (n=3) levels following the transfection of BMECs with p23 siRNA. (F) mRNA expression levels of ACSL4 in BMECs following p23 siRNA transfection (n=3). (G) Western blot analysis of GPX4 in BMECs following p23 siRNA transfection and (H) statistical analysis (n=3). (I) mRNA expression levels of SLC7A11 in BMECs following p23 siRNA transfection (n=3). Intracellular (J) GSH (n=3), (K) MDA (n=3) and (L) ROS (n=3) levels in BMECs with p23 OE. (M) Western blot analysis of GPX4 and (N) statistical analysis in BMECs with p23 OE (n=3). mRNA expression levels of (O) SLC7A11 (n=3) and (P) ACSL4 (n=3) in BMECs with p23 OE. Data are presented as the mean ± SD. *P<0.05, **P<0.01, ***P<0.001 and ****P<0.0001. CCK, Cell Counting Kit; OGD/R, oxygen-glucose deprivation/reoxygenation; BMECs, brain microvascular endothelial cells; GSH, glutathione; MDA, malondialdehyde; ROS, reactive oxygen species; ACSL4, acyl-CoA synthetase long-chain family member 4; GPX4, glutathione peroxidase 4; SLC7A11, subunit solute carrier family 7 member 11; COX-2, cyclooxygenase-2; OE, overexpression; siRNA, small interfering RNA; NC, negative control; RSL3, RAS-selective lethal 3; ns, not significant.

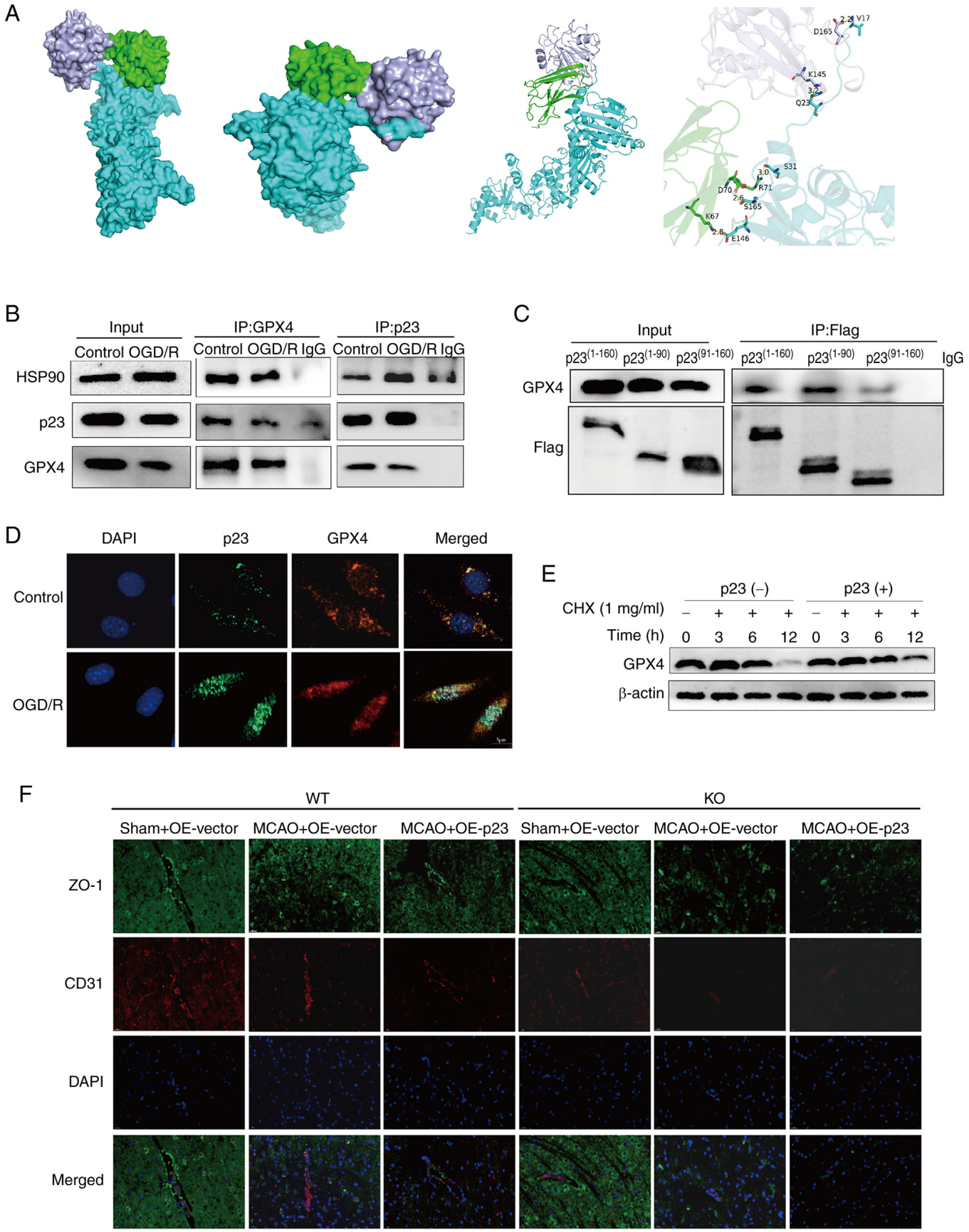

Figure 6. GPX4 mediates the protective effect of p23 on ferroptosis in BMECs. (A) Protein docking mimicking the interaction between p23 (green), GPX4 (violet) and HSP90 (cyan). (B) Interaction between p23, GPX4 and HSP90 was detected using co-immunoprecipitation. (C) Structural domain of p23 interacting with GPX4 was detected using co-immunoprecipitation. (D) Co-localization of p23 and GPX4 was detected using immunofluorescence (magnification, x400). (E) Effect of p23 on the stability of the GPX4 protein. (F) Expression of ZO-1 in GPX4 $Fos^{CreERT2}$ mice following p23 overexpression was detected using immunofluorescence (magnification, x100). BMECs, brain microvascular endothelial cells; GPX4, glutathione peroxidase 4; HSP90, heat shock protein 90; ZO-1, zonula occludens-1; CHX, cycloheximide.

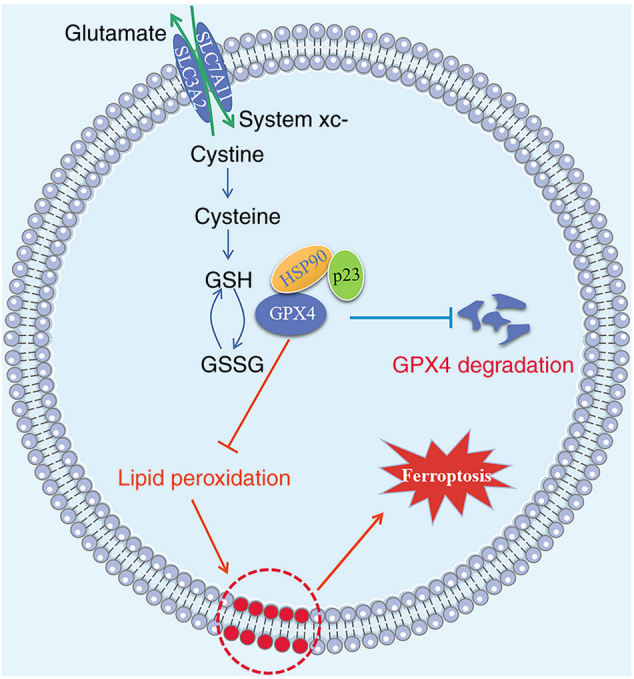

Figure 7. p23 protects against ferroptosis of BMECs in ischemic stroke. p23 was significantly upregulated following stroke-like conditions in *in vitro* and *in vivo* models, and formed a complex with HSP90 and GPX4 through its N-terminal structure (1-90aa), which improved their stability, inhibited GPX4 degradation, and ultimately inhibited ferroptosis in BMECs, thereby protecting against ischemia/reperfusion-induced blood-brain barrier injury. BMECs, brain microvascular endothelial cells; GSH, glutathione; GPX4, glutathione peroxidase 4; HSP90, heat shock protein 90.

tested. The results showed that the stability of GPX4 protein was markedly increased following p23 OE (Fig. 6E). To further verify the experimental results, GPX4 $Fos^{CreERT2}$ mice were used to construct a model of MCAO. The results showed that the reduction of ZO-1 in GPX4 $Fos^{CreERT2/-}$ mice in the MCAO model was partially reversed by p23 OE, while p23 OE did not have this effect on GPX4 $Fos^{CreERT2/+}$ mice (Fig. 6F); CD31 was used to indicate the location of blood vessels, indicating that p23 may have a protective role by regulating ferroptosis through GPX4. The present findings demonstrated that p23 may form complexes with HSP90 and GPX4 through its N-terminal domain (1-90aa), thus enhancing the stability of GPX4, inhibiting the degradation of GPX4 and ultimately inhibiting BMEC ferroptosis, thereby protecting against cerebral I/R-induced BBB damage.

Discussion

The present study illustrated the crucial role of p23 as a key regulator of BBB injury following CIRI. First, p23 was revealed to be markedly upregulated under stroke-like conditions in both *in vitro* and *in vivo* models. p23 also formed a complex with HSP90 and GPX4 through its N-terminal structure (1-90aa), which improved their stability, inhibited GPX4 degradation, and ultimately inhibited ferroptosis in BMECs, thereby protecting against I/R-induced BBB injury. The aforementioned results are shown in Fig. 7. These findings may have important implications for potential future stroke treatment or prevention.

Ischemic stroke is the leading cause of death and long-term disability worldwide, and reperfusion after ischemia can trigger a series of harmful events, among which BBB disruption is one of the most critical indicators (27). TJs are complexes formed between microvascular endothelial cells, and their function is especially crucial for maintaining the integrity of the BBB. When TJs open, the integrity of the BBB is undermined. TJs are composed of a complex network of proteins, such as occludin, claudin and ZO-1, -2 and -3. Among them, occludin and ZO-1 have been discovered to be particularly significant in the assembly of endothelial cell connections that sustain the BBB, and their loss is associated with disruption of the BBB (28,29). Ferroptosis is a novel iron-dependent form of regulated cell death that differs in genetics, morphology and biochemistry from apoptosis, autophagy and necrotic cell death (9). Notably, it has been discovered to serve an important role in BBB dysfunction (10,14,30). In line with previous reports, the present results showed that cerebral I/R may lead to BBB injury and increased BBB permeability. *In vitro*, OGD/R led to BMEC damage and decreased the expression of TJ proteins ZO-1 and occludin. In addition, rats were pretreated with an intracerebroventricular injection of Fer-1 and a MCAO model was established. The results indicated that Fer-1 markedly enhanced ZO-1 expression. *In vitro*, the level of lipid peroxidation in BMECs rose significantly, and the antioxidant content was markedly decreased following OGD/R treatment, indicating that ferroptosis may participate in OGD/R-induced BMEC injury.

Ferroptosis has become a global research focus. The co-chaperone p23 is also known as cytosolic prostaglandin E (PGE) synthase (15), and the COX-2/PGE2 pathway has been reported to be closely associated with CIRI (31). p23 is involved in PGE2 synthesis, and there is evidence suggesting a connection between the COX-2/PGE2 pathway and ferroptosis (32). Recent studies have shown that PGE2 can prevent CIRI-induced ferroptosis (13,33), but the specific mechanism requires further exploration. In the present study, *in vitro* experiments showed that p23 knockdown promoted OGD/R-induced ferroptosis in BMECs, and further aggravated I/R-induced BBB damage. After OE of p23, the occurrence of ferroptosis in BMECs could be inhibited and BBB damage could be improved. These results indicated that p23 may exert a protective effect by regulating GPX4.

The biochemical mechanism of ferroptosis involves the iron-dependent formation of lipid-ROS, and consumption of GSH or inactivation of GPX4 (34,35). Phospholipid hydroperoxide is an enzyme that reduces phospholipid hydroperoxides to the corresponding phospholipid alcohol, and its expression or activity is regulated by selenium and GSH (36). In the course of the present study, it was discovered that the expression levels of GPX4 were regulated by p23, suggesting that p23 may regulate ferroptosis by targeting GPX4. To further prove this, the effect of p23 on GPX4 protein stability was assessed, and it was demonstrated that GPX4 protein stability was markedly increased following p23 OE. In GPX4 $Fos^{CreERT2/+}$ mice, p23 almost lost the ability to increase the expression of ZO-1, suggesting that GPX4 is an important site for p23 to serve a protective role in BBB. p23 often plays a unique biological function as a molecular chaperone and serves a regulatory role in a variety of diseases by binding to a various protein to regulate

their biological function. First, it is an important co-molecular chaperone of HSP90, assisting HSP90 in completing its molecular chaperone function through its C-terminal co-chaperone complex (37). Genome and proteomics screening in yeast has revealed a network showing that p23 may have an HSP90-independent effect in intracellular receptor-regulated gene expression, and shows the characteristics of ribosomal biogenesis and vesicle-mediated transport (18,38). Through immunofluorescence co-localization experiments, the present study revealed that p23 co-localizes with GPX4 in cells. Further verification by protein docking and co-immunoprecipitation experiments showed that p23 forms a complex with HSP90 and GPX4 through its N-terminal domain (1-90aa) and enhances the stability of GPX4, inhibits the degradation of GPX4 and ultimately inhibits ferroptosis in BMECs, protecting against I/R-induced BBB injury. To the best of our knowledge, the present study was the first to explore the mechanism of p23 regulating ferroptosis in BMECs to protect against BBB dysfunction, providing hope for future clinical applications and laying the foundation for more effective stroke treatment by protecting against BBB damage.

There are some limitations in the current study. Although the OE of p23 did not significantly change protein expression levels in the control group, there was a significant difference in the OGD/R group, as well as in the mRNA levels of p23 in the control group. It could be hypothesized that this may be due to the fact that in the control group, after p23 is overexpressed, cells may counteract functional activation by downregulating the protein level of p23, thus achieving homeostasis of the body, while in the OGD/R group, the destruction of homeostasis led to effective OE.

In conclusion, p23 exerts a protective effect against cerebral I/R-induced BBB injury by suppressing the ferroptosis of BMECs through enhancing the stability of GPX4, offering a potential therapeutic target for ischemic stroke.

Acknowledgements

Not applicable.

Funding

This work was funded by the National Natural Science Foundation of China (grant nos. 82172147, 81571880, 81373147, 30901555 and 30972870) and the Natural Science Foundation of Hunan Province (grant nos. 2021JJ30900 and 2016JJ2157). All these funding bodies supported the study design, data collection, analysis, interpretation and manuscript writing.

Availability of data and materials

The data generated in the present study may be requested from the corresponding author.

Authors' contributions

YL and JZ designed and guided the project. YZ and YX conducted the experiments. YZ, YX, QX and NH analyzed the data. All authors discussed the results and contributed to the final version of the manuscript. YZ and YX wrote the manuscript. YL and JZ revised the manuscript. YL is the principal corresponding author and is responsible for the integrity of the work in its entirety from its initiation to the publication of the article. YL and JZ confirm the authenticity of all the raw data. All authors read and approved the final version of the manuscript.

Ethics approval and consent to participate

All the procedures carried out in studies involving animals were in line with the ethical standards of the institution or practice where the studies were conducted, and were approved by the Experimental Animal Center of Central South University (Changsha, China; approval no. 2018sydw0222).

Patient consent for publication

Not applicable.

Competing interests

The authors declare that they have no competing interests.

References

1. Miller JB, Merck LH, Wira CR, Meurer WJ, Schrock JW, Nomura JT, Siket MS, Madsen TE, Wright DW, Panagos PD and Lewandowski C: The advanced reperfusion Era: Implications for emergency systems of ischemic stroke care. Ann Emerg Med 69: 192-201, 2017.
2. Eltzschig HK and Eckle T: Ischemia and reperfusion-from mechanism to translation. Nat Med 17: 1391-1401, 2011.
3. Leigh R, Christensen S, Campbell BC, Marks MP, Albers GW and Lansberg MG: Pretreatment blood-brain barrier disruption and post-endovascular intracranial hemorrhage. Neurology 87: 263-269, 2016.
4. Jiang X, Andjelkovic AV, Zhu L, Yang T, Bennett MVL, Chen J, Keep RF and Shi Y: Blood-brain barrier dysfunction and recovery after ischemic stroke. Prog Neurobiol 163-164: 144-171, 2018.
5. Leigh R, Jen SS, Hillis AE, Krakauer JW and Barker PB: Pretreatment blood-brain barrier damage and post-treatment intracranial hemorrhage in patients receiving intravenous tissue-type plasminogen activator. Stroke 45: 2030-2035, 2014.
6. Desilles JP, Rouchaud A, Labreuche J, Meseguer E, Laissy JP, Serfaty JM, Lapergue B, Klein IF, Guidoux C, Cabrejo L, *et al*: Blood-brain barrier disruption is associated with increased mortality after endovascular therapy. Neurology 80: 844-851, 2013.
7. Villringer K, Sanz Cuesta BE, Ostwaldt AC, Grittner U, Brunecker P, Khalil AA, Schindler K, Eisenblätter O, Audebert H and Fiebach JB: DCE-MRI blood-brain barrier assessment in acute ischemic stroke. Neurology 88: 433-440, 2017.
8. Ji B, Zhou F, Han L, Yang J, Fan H, Li S, Li J, Zhang X, Wang X, Chen X and Xu Y: Sodium Tanshinone IIA sulfonate enhances effectiveness Rt-PA treatment in acute ischemic stroke patients associated with ameliorating blood-brain barrier damage. Transl Stroke Res 8: 334-340, 2017.
9. Dixon SJ, Lemberg KM, Lamprecht MR, Skouta R, Zaitsev EM, Gleason CE, Patel DN, Bauer AJ, Cantley AM, Yang WS, *et al*: Ferroptosis: An iron-dependent form of nonapoptotic cell death. Cell 149: 1060-1072, 2012.
10. Zhao Y, Liu Y, Xu Y, Li K, Zhou L, Qiao H, Xu Q and Zhao J: The role of ferroptosis in blood-brain barrier injury. Cell Mol Neurobiol 43: 223-236, 2022.
11. Tuo QZ, Lei P, Jackman KA, Li XL, Xiong H, Li XL, Liuyang ZY, Roisman L, Zhang ST, Ayton S, *et al*: Tau-mediated iron export prevents ferroptotic damage after ischemic stroke. Mol Psychiatry 22: 1520-1530, 2017.
12. Yan BC, Cao J, Liu J, Gu Y, Xu Z, Li D and Gao L: Dietary Fe3O4 Nanozymes prevent the injury of neurons and blood-brain barrier integrity from cerebral ischemic stroke. ACS Biomater Sci Eng 7: 299-310, 2021.

13. Xu Y, Li K, Zhao Y, Zhou L, He N, Qiao H, Xu Q, Zhang H, Liu Y and Zhao J: Inhibition of 15-hydroxyprostaglandin dehydrogenase protects neurons from ferroptosis in ischemic stroke. MedComm 5: e452, 2024.
14. Liu H, Hua Y, Keep RF and Xi G: Brain ceruloplasmin expression after experimental intracerebral hemorrhage and protection against Iron-induced brain injury. Transl Stroke Res 10: 112-119, 2019.
15. Tanioka T, Nakatani Y, Semmyo N, Murakami M and Kudo I: Molecular identification of cytosolic prostaglandin E2 synthase that is functionally coupled with cyclooxygenase-1 in immediate prostaglandin E2 biosynthesis. J Biol Chem 275: 32775-32782, 2000.
16. Exner KS and Ivanova A: A doxorubicin-peptide-gold nanoparticle conjugate as a functionalized drug delivery system: Exploring the limits. Phys Chem Chem Phys 24: 14985-14992, 2022.
17. Martinez-Yamout MA, Venkitakrishnan RP, Preece NE, Kroon G, Wright PE and Dyson HJ: Localization of sites of interaction between p23 and Hsp90 in solution. J Biol Chem 281: 14457-14464, 2006.
18. Echtenkamp FJ, Zelin E, Oxelmark E, Woo JI, Andrews BJ, Garabedian M and Freeman BC: Global functional map of the p23 molecular chaperone reveals an extensive cellular network. Mol Cell 43: 229-241, 2011.
19. Grad I, McKee TA, Ludwig SM, Hoyle GW, Ruiz P, Wurst W, Floss T, Miller CA III and Picard D: The Hsp90 cochaperone p23 is essential for perinatal survival. Mol Cell Biol 26: 8976-8983, 2006.
20. Lovgren AK, Kovarova M and Koller BH: cPGES/p23 is required for glucocorticoid receptor function and embryonic growth but not prostaglandin E2 synthesis. Mol Cell Biol 27: 4416-4430, 2007.
21. Patwardhan CA, Fauq A, Peterson LB, Miller C, Blagg BS and Chadli A: Gedunin inactivates the co-chaperone p23 protein causing cancer cell death by apoptosis. J Biol Chem 288: 7313-7325, 2013.
22. Livak KJ and Schmittgen TD: Analysis of relative gene expression data using real-time quantitative PCR and the 2(-Delta Delta C(T)) method. Methods 25: 402-408, 2001.
23. Liu WY, Wang ZB, Zhang LC, Wei X and Li L: Tight junction in blood-brain barrier: An overview of structure, regulation, and regulator substances. CNS Neurosci Ther 18: 609-615, 2012.
24. Liu H, Zhang TA, Zhang WY, Huang SR, Hu Y and Sun J: Rhein attenuates cerebral ischemia-reperfusion injury via inhibition of ferroptosis through NRF2/SLC7A11/GPX4 pathway. Exp Neurol 369: 114541, 2023.
25. Xiao P, Huang H, Zhao H, Liu R, Sun Z, Liu Y, Chen N and Zhang Z: Edaravone dexborneol protects against cerebral ischemia/reperfusion-induced blood-brain barrier damage by inhibiting ferroptosis via activation of nrf-2/HO-1/GPX4 signaling. Free Radic Biol Med 217: 116-125, 2024.
26. Yu Z, Peng Y, Gao J, Zhou M, Shi L, Zhao F, Wang C, Tian X, Feng L, Huo X, *et al*: The p23 co-chaperone is a succinate-activated COX-2 transcription factor in lung adenocarcinoma tumorigenesis. Sci Adv 9: eade0387, 2023.
27. Neuwelt EA, Bauer B, Fahlke C, Fricker G, Iadecola C, Janigro D, Leybaert L, Molnár Z, O'Donnell ME, Povlishock JT, *et al*: Engaging neuroscience to advance translational research in brain barrier biology. Nat Rev Neurosci 12: 169-182, 2011.
28. Hawkins BT and Davis TP: The blood-brain barrier/neurovascular unit in health and disease. Pharmacol Rev 57: 173-185, 2005.
29. Zlokovic BV: The blood-brain barrier in health and chronic neurodegenerative disorders. Neuron 57: 178-201, 2008.
30. Rand D, Ravid O, Atrakchi D, Israelov H, Bresler Y, Shemesh C, Omesi L, Liraz-Zaltsman S, Gosselet F, Maskrey TS, *et al*: Endothelial iron homeostasis regulates Blood-brain barrier integrity via the HIF2α-Ve-cadherin pathway. Pharmaceutics 13: 311, 2021.
31. Xu Y, Liu Y, Li K, Miao S, Lv C, Wang C and Zhao J: Regulation of PGE2 pathway during cerebral ischemia reperfusion injury in rat. Cell Mol Neurobiol 41: 1483-1496, 2021.
32. Chen B, Chen Z, Liu M, Gao X, Cheng Y, Wei Y, Wu Z, Cui D and Shang H: Inhibition of neuronal ferroptosis in the acute phase of intracerebral hemorrhage shows long-term cerebroprotective effects. Brain Res Bull 153: 122-132, 2019.
33. Xu Y, Liu Y, Li K, Yuan D, Yang S, Zhou L, Zhao Y, Miao S, Lv C and Zhao J: COX-2/PGE2 pathway inhibits the ferroptosis induced by cerebral ischemia reperfusion. Mol Neurobiol 59: 1619-1631, 2022.
34. Zou Y, Li H, Graham ET, Deik AA, Eaton JK, Wang W, Sandoval-Gomez G, Clish CB, Doench JG and Schreiber SL: Cytochrome P450 oxidoreductase contributes to phospholipid peroxidation in ferroptosis. Nat Chem Biol 16: 302-309, 2020.
35. Yang WS, Kim KJ, Gaschler MM, Patel M, Shchepinov MS and Stockwell BR: Peroxidation of polyunsaturated fatty acids by lipoxygenases drives ferroptosis. Proc Natl Acad Sci USA 113: E4966-E4975, 2016.
36. Friedmann Angeli JP and Conrad M: Selenium and GPX4, a vital symbiosis. Free Radic Biol Med 127: 153-159, 2018.
37. Daneri-Becerra C, Valeiras B, Gallo LI, Lagadari M and Galigniana MD: Cyclophilin A is a mitochondrial factor that forms complexes with p23-correlative evidence for an anti-apoptotic action. J Cell Sci 134, 2021.
38. Freeman BC, Felts SJ, Toft DO and Yamamoto KR: The p23 molecular chaperones act at a late step in intracellular receptor action to differentially affect ligand efficacies. Genes Dev 14: 422-434, 2000.